AIAA JOURNAL
Vol. 39, No. 8, August 2001

Structural Design Optimization of Nonlinear Symmetric Structures Using the Group Theoretic Approach

R. Sedaghati,* B. Tabarrok,† and A. Suleman‡
University of Victoria, Victoria, British Columbia V8W 3P6, Canada

Among multidisciplinary analysis and optimization problems, structural optimization of geometrically nonlinear stability problems is of great importance, especially in structures used in space applications, because of their long and slender configurations. In this study, application of the group theoretic approach (GTA) in structural optimization of geometrical nonlinear problems under system stability constraint has been investigated. According to GTA, the number of displacement degrees of freedom in the initial configuration can be reduced significantly by using the set of symmetry transformations of the undeformed structure to construct a projection matrix from full space to a reduced subspace spanned by the symmetry modes. A structural optimization algorithm is developed for shallow structures undergoing large deflections subject to system stability constraint. The method combines the nonlinear buckling analysis, based on the displacement control technique using GTA, with the optimality criteria approach, based on the potential energy of the system. A shallow dome truss structure has been designed to illustrate the proposed methodology. This paper demonstrates that structural optimization of nonlinear symmetric structures using GTA is computationally efficient, and excellent agreement exists between optimal results in full space and those in the reduced subspace. Also, it is shown that structural design based on the generalized eigenvalue problem (linear buckling) highly underestimates the optimum mass, which may lead to structural failure.

Introduction

FOR optimum structural design, the design variables are selected so as to minimize the weight of the structure while satisfying all of the constraints. The constraints may include maximum allowable stresses in the elements, displacement limits at the joints, frequency specifications, system stability, and so forth. Depending on the nature of the applied loads, the structure, and its geometry, one or more of the constraints can be active and control the design of the structure. The design variables will generally be dictated by the dominant constraints. In most previous works (e.g., Refs. 1–4) the system stability requirement is posed as a linear buckling analysis. Linear analysis is restricted to small rotations and equilibrium in the initial state. Linear buckling reduces to the solution of a generalized eigenvalue problem for the buckling loads (bifurcation point). This definition of system stability for some structures may not be conservative enough, because the nonlinear behavior of the structure will result in large changes in the geometry of the structure. Furthermore, the presence of geometric imperfections affects the structural response more significantly in large deflection analysis. For this reason, a nonlinear buckling analysis should be undertaken to find the more conservative buckling loads (limit point).

In optimization of structures undergoing large deflections, finding the exact limit point is critical for defining a nonlinear buckling constraint. In the past works, the finite element analysis based on a load control technique[5–7] has been used to trace the nonlinear load-deflection curve for determination of the limit load. For a simple two-bar truss structure, an exact formulation that includes the conditions for instability and optimality has been developed by different investigators.[8,9] Techniques using load control fail as the load approaches the buckling load, or requires extremely small increments to carry out the analysis, or needs sophisticated techniques such as automatic time stepping and arc-length method. Several procedures have been used by different investigators to overcome this difficulty. Zienkiewicz[10] and Thomas and Gallager[11] suggested a form of the displacement control method. Their algorithm requires modifications of the stiffness matrix. Haisler et al.[12] used that method by partitioning the stiffness matrix. Helpful simplifications to the displacement control method were made by Batoz and Dhatt,[13] where one of the displacement components is incremented at each time step and an iterative process is followed: that is, a dominant displacement component is chosen as an independent variable instead of the usual loading parameter. Using this approach, symmetry and banded properties of the stiffness matrix are preserved. The displacement control technique proposed by Batoz and Dhatt has been used as an analyzer in the optimum design of truss structures undergoing large deflections subject to the system stability constraint.[14,15] The method was found to be extremely efficient in optimizing the structures under snap-through buckling load.

The displacement control technique proposed by Batoz and Dhatt[13] has been used in this investigation to capture the limit point in problem with nonlinear buckling constraints. Using a quadratic fit to the load-displacement curve near the critical load, the limit load has been obtained efficiently and accurately.

Most methods used to solve static nonlinear problems are based on Newton–Raphson or quasi-Newton methods.[16] For a structure with m displacement degrees of freedom (DOF), these methods require the solution of m simultaneous equations, respectively. Therefore, when the number of DOF is large, these methods can become computationally expensive. For the special case of structural systems with symmetry, it has recently been shown that a nonlinear solution can be computed exactly using a reduction technique based on symmetry modes called the group theoretic approach (GTA). The essence of the reduction technique is to reduce the number of DOF in the initial configuration by transforming a large system to a similar, much smaller, substitute system. In other words, the number of DOF in the large system m is much larger than the number of DOF in the reduced problems, m_r. The response $\boldsymbol{U}$ of the large system can be obtained by a combination of a few subspace modes or basis vectors. This is accomplished by expressing $\boldsymbol{U}$ as a product of a transformation matrix Φ and the response $\boldsymbol{U}_r$ of the reduced problem. By mapping the displacement vector from the symmetry subspace back to the full space for the calculation of internal forces, the GTA guarantees the satisfaction of equilibrium equations in the full space.

The group theoretic foundations of the reduction method have been presented by Healey.[17–19] Using the projection operator of group theory explained by Miller,[20] Healey has described, within the general setting of symmetric problems in structural mechanics, how to form a dimensionally reduced problem leading to significant

Received 7 February 2000; revision received 1 September 2000; accepted for publication 5 September 2000.

*Ph.D. Student, Department of Mechanical Engineering, P.O. Box 3055.
†Professor, Department of Mechanical Engineering, P.O. Box 3055.
‡Associate Professor, Instituto de Engenharia Mecanica (IDMEC). Member AIAA.

computational savings. This technique has been applied to electrostatics and bifurcation problems. Subsequently, Chang and Healey[21] used the GTA in analysis of a geometrically nonlinear system with symmetry. More recently, Li[22] solved for static and dynamic analysis of nonlinear problems with symmetry using the GTA. However, nonlinear buckling analysis and postbuckling behavior have not been considered in all of the previous reported studies using the GTA. This paper addresses this issue and illustrates its application on a shallow dome structure. The application of the GTA in the structural optimization of the nonlinear problems under system stability constraint is introduced for the first time.

The optimum solution of the nonlinear buckling problems under system stability constraint by general mathematical programming algorithms is computationally inefficient because of the many iterations and sensitivity analyses required.[23,24] This difficulty can be alleviated by the optimality criterion method. Here an optimality criterion algorithm based on the potential energy has been used.[5,14] The Lagrange multipliers are obtained in a closed-form solution. Thus, no recurrence relation has been used for updating the Lagrange multipliers. This procedure enables us to obtain the optimum solution with an infeasible starting point.

In the following sections, a short description of the nonlinear analysis procedure is presented. This is followed by a description of the GTA. The derivation of the optimality criterion and the recurrence relations are given next. Finally, a complex, shallow, dome structure is optimized using both nonlinear and linear buckling analyses. For a shallow dome subjected to a concentrated apex load, the system stability is the important active constraint and design driver. It is shown that the structural optimization of the nonlinear problems under system stability constraint using the GTA can significantly reduce the computational time with excellent agreement between the subspace and full-space optimal solutions. Furthermore, it has also been shown that optimization of nonlinear structures using linear buckling analysis underestimates the optimum mass of the structures (or overestimates the buckling load), which may lead to structural failure.

Nonlinear Analysis

In the presence of large deflections, geometrical nonlinearity becomes important. In such cases, although the strains are small and the material behaves linearly, the response of the structure becomes nonlinear as a result of finite rotations and displacements. It is therefore necessary to write the joint equilibrium in terms of the final geometry of the structure. In the case of large displacements, the strain–displacement relationships include nonlinear terms. Consideration of these terms, using the principle of virtual work, the system stiffness matrix can be obtained and written as

$$\boldsymbol{K} = \boldsymbol{K}_E + \boldsymbol{K}_G \tag{1}$$

where $\boldsymbol{K}$ is the system tangent stiffness matrix, $\boldsymbol{K}_E$ is the system linear elastic stiffness matrix, and $\boldsymbol{K}_G$ is the system geometric stiffness matrix. The matrix $\boldsymbol{K}_G$ is associated with the changes in the geometry of the structure. These matrices are obtained by the assemblage of the element linear elastic and geometric stiffness matrices in the global coordinates.

To derive the incremental finite element equations, it is assumed that the equilibrium configuration at a load level is known and the configuration at a slightly higher load level is to be determined. Using the Newton–Raphson method, these equations may be written[13,16] as

$$^{t+\Delta t}\boldsymbol{K}^{(k-1)}\Delta\boldsymbol{U}^{(k)} = \Delta\boldsymbol{P}^{(k-1)} = {}^{t+\Delta t}\alpha^{(k)}\boldsymbol{P}_{\text{ref}} - {}^{t+\Delta t}\boldsymbol{P}'^{(k-1)}$$

$$^{t+\Delta t}\boldsymbol{U}^{(k)} = {}^{t+\Delta t}\boldsymbol{U}^{(k-1)} + \Delta\boldsymbol{U}^{(k)} \tag{2}$$

where k is the iteration number, $^{t+\Delta t}\boldsymbol{K}$ is the tangent stiffness matrix at time step $t+\Delta t$, $^{t+\Delta t}\boldsymbol{P}'^{(k-1)}$ is the vector of the nodal resultant member forces at time step $t+\Delta t$, $\boldsymbol{P}_{\text{ref}}$ is a given reference load, $^{t+\Delta t}\alpha$ is a load factor parameter to denote the external load at time step $t+\Delta t$, $\Delta\boldsymbol{P}$ is the out-of-balance force, $\Delta\boldsymbol{U}$ is the vector of increments in nodal displacements, and $^{t+\Delta t}\boldsymbol{U}$ is the vector of nodal displacement at time step $t+\Delta t$. The out-of-balance load vector

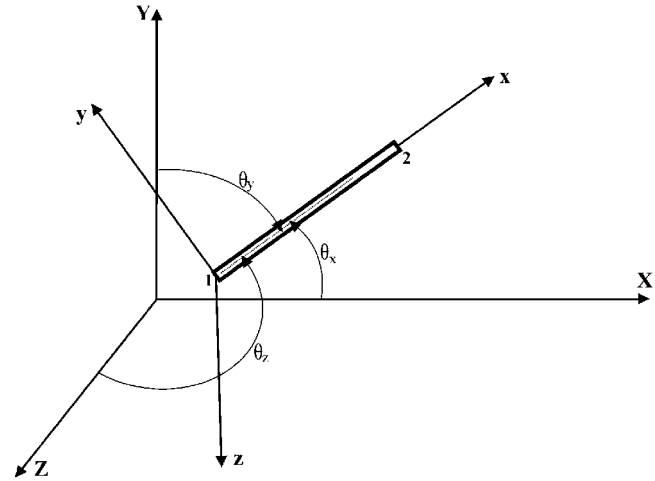

Fig. 1 Two-node space truss element.

$\Delta\boldsymbol{P}$ corresponds to a load vector that is not yet balanced by element forces, and hence an increment in the nodal displacements is required. This updating of the nodal displacements in the iteration is continued until the out-of-balance loads and incremental displacements are small. To guarantee that both out-of-balance loads and incremental displacements are small, the energy convergence criteria[16] (a product of out-of-balance force and incremental displacement) have been used in this analysis. An energy convergence tolerance of $\varepsilon_E = 10^{-6}$ has been selected in this analysis.

It is noted that the increment in load or displacement is conventionally represented as an evolution in time t. The problem is static, and t simply denotes incremental steps in the solution.

For a truss element, shown in Fig. 1, $\boldsymbol{K}_E$ and $\boldsymbol{K}_G$ in global coordinates are as follows[17]:

$$\boldsymbol{K}_E = \frac{AE}{L}\begin{bmatrix} \bar{\boldsymbol{K}}_E & -\bar{\boldsymbol{K}}_E \\ -\bar{\boldsymbol{K}}_E & \bar{\boldsymbol{K}}_E \end{bmatrix}, \qquad \boldsymbol{K}_G = \frac{F}{L}\begin{bmatrix} \boldsymbol{I} & -\boldsymbol{I} \\ -\boldsymbol{I} & \boldsymbol{I} \end{bmatrix} \tag{3}$$

where

$$\bar{\boldsymbol{K}}_E = \begin{bmatrix} l_x^2 & l_x l_y & l_x l_z \\ l_x l_z & l_y^2 & l_y l_z \\ l_x l_z & l_y l_z & l_z^2 \end{bmatrix}, \qquad \boldsymbol{I} = \begin{bmatrix} 1 & 0 & 0 \\ 0 & 1 & 0 \\ 0 & 0 & 1 \end{bmatrix}, \qquad \begin{aligned} l_x &= \cos\theta_x \\ l_y &= \cos\theta_y \\ l_z &= \cos\theta_z \end{aligned} \tag{4}$$

where F is the axial force in the element at time t; A is the cross-sectional area of the element; L the length of the element; E is the Young's modulus; and l_x, l_y, and l_z are the direction cosines of the element x axis relative to the global X, Y, and Z axes, respectively.

In the displacement control method, the external load during iteration in a particular time step does not remain constant. In other words, for each increment in a controlling displacement component, the load is assumed to vary so that the multiplication of the out-of-balance load vector and the incremental displacement vector become as small as desired. Because the displacement control method traces the postbuckling path, one can estimate the peak load by very small displacement increments. The true peak load is the largest load obtained as the displacement traces the equilibrium path. However, the solution obtained is sensitive to the displacement increments employed and the cost of the accurate solution becomes prohibitive. Here, the peak load is obtained by performing a quadratic fit to the load-displacement curve near the critical load and finding the maximum of this curve. The peak load determined using this procedure was found to be very accurate, and it is not sensitive to the displacement increments.

Nonlinear Analysis of Symmetric Structures Using the GTA

In general, a nonlinear equation can be written symbolically as

$$f(\boldsymbol{U}, \boldsymbol{P}) = \boldsymbol{K}\boldsymbol{U} - \boldsymbol{P} = 0 \tag{5}$$

Let us suppose that Eq. (5) represents a structure with m DOF and with undeformed geometry (shape), material properties and geometric boundary conditions having common, nontrivial symmetry. Symmetry is characterized mathematically by an isometric (strain-free) transformation of the undeformed structure into a completely equivalent configuration. The set of all such isometries $\boldsymbol{G} \ldots \{\boldsymbol{G}_1, \boldsymbol{G}_2, \ldots, \boldsymbol{G}_N\}$; $\boldsymbol{G}_i \lfloor \sum^{3 \leftrightarrow 3}$ is called the symmetry group of the structure. For finite structural systems, the relevant isometries are all $3 \leftrightarrow 3$ orthogonal matrices corresponding to rotations, reflections, and inversion.[20] An orthogonal representation of a symmetric group of $\boldsymbol{G}$ on m-dimensional space is $\boldsymbol{T} \ldots \{\boldsymbol{T}_1, \boldsymbol{T}_2, \ldots, \boldsymbol{T}_N\}$; $\boldsymbol{T}_i \lfloor \sum^{m \leftrightarrow m}$, named rep of $\boldsymbol{G}$ on $\sum^{m \leftrightarrow m}$ and it satisfies the following properties:

$$\boldsymbol{T}(\boldsymbol{G}_1)\boldsymbol{T}(\boldsymbol{G}_2) = \boldsymbol{T}(\boldsymbol{G}_1\boldsymbol{G}_2) \text{ for all } \boldsymbol{G}_1, \boldsymbol{G}_2 \lfloor \boldsymbol{G}$$

$$\boldsymbol{T}^T(\boldsymbol{G}_1) = \boldsymbol{T}\left(\boldsymbol{G}_1^T\right), \boldsymbol{T}^{-1}(\boldsymbol{G}_1) = \boldsymbol{T}\left(\boldsymbol{G}_1^{-1}\right) \text{ for all } \boldsymbol{G}_1 \lfloor \boldsymbol{G}$$

$$\boldsymbol{T}(\boldsymbol{I}) = \boldsymbol{I}, \text{ where } \boldsymbol{I} \text{ is the } (m \leftrightarrow m) \text{ identity matrix}$$

The equilibrium equations of symmetric models such as Eq. (5) can reflect the symmetry of the mechanical or physical system through a property called the equivariance.[18] Equation (5) is said to be equivariant under the action of $\boldsymbol{T}$ if

$$\boldsymbol{f}(\boldsymbol{TU}, \boldsymbol{P}) = \boldsymbol{Tf}(\boldsymbol{U}, \boldsymbol{P}) \tag{6}$$

The equivariance condition in Eq. (6) follows from the fact that the loading, the material properties, and the boundary conditions agree with the geometric symmetry of the structure. If any of these has less symmetry than the purely geometric symmetry, then an appropriate subgroup must be employed.

A symmetric solution to Eq. (6) is a nodal displacement vector $\boldsymbol{U}^*$ and a load magnitude $\boldsymbol{P}^*$ satisfying equilibrium such that $\boldsymbol{TU}^* = \boldsymbol{U}^*$. It can be shown[20] that the average matrix

$$\boldsymbol{Pr} = \frac{1}{N}\sum_{i=1}^{N} \boldsymbol{T}_i \tag{7}$$

is a symmetric ($\boldsymbol{Pr}^T = \boldsymbol{Pr}$) projection ($\boldsymbol{PrPr} = \boldsymbol{Pr}$) onto the subspace $\boldsymbol{U}_s | \Sigma^m$ of all symmetric displacement fields ($\boldsymbol{U}^*$) and is called the projection matrix. If the $\boldsymbol{m}$ vector ϕ is in $\boldsymbol{U}_s$ then

$$\boldsymbol{Pr}\phi = \phi \tag{8}$$

where ϕ is an eigenvector of $\boldsymbol{Pr}$ corresponding to the unit eigenvalue. It can also be shown[20] that the dimension of $\boldsymbol{U}_s$ is given by

$$m_r = \text{trace}(\boldsymbol{Pr}) = \frac{1}{N}\sum_{i=1}^{N} \text{trace}(\boldsymbol{T}_i) \tag{9}$$

Hence, the multiplicity of the unit eigenvalue in Eq. (8) is equal to m_r. The most useful way to construct a reduced problem is to determine the basis for $\boldsymbol{U}_s$ as

$$\Phi = \{\phi_1, \phi_2, \ldots, \phi_{m_r}\}, \qquad \text{where} \qquad \phi_i^T \phi_j = \delta_{ij} \tag{10}$$

These basis vectors $\phi_i, i = 1, 2, \ldots, m_r$, which are solutions to Eq. (8), are called symmetry modes. The matrix Φ including the symmetry modes is a $\boldsymbol{m} \leftrightarrow \boldsymbol{m}_r$ matrix. If displacement vector $\boldsymbol{U}$ is in $\boldsymbol{U}_s$ (symmetric solution $\boldsymbol{U}^*$), then

$$\boldsymbol{U}_r = \Phi^T \boldsymbol{U} \tag{11}$$

is an $\boldsymbol{m}_r$ vector with entries corresponding to the components of $\boldsymbol{U}$ relative to the basis $\{\phi_1, \phi_2, \ldots, \phi_{m_r}\}$, that is, $\boldsymbol{U}_{\text{ri}} = \phi_i^T \boldsymbol{U}, i = 1, 2, \ldots, \boldsymbol{m}_r$. From Eq. (11), we can write

$$\boldsymbol{U} = \Phi \boldsymbol{U}_r \tag{12}$$

Considering Eq. (12) in Eq. (5) and multiplying both sides by Φ^T, the reduced problem may be given explicitly by

$$\Phi^T f(\Phi \boldsymbol{U}_r, \boldsymbol{P}) = \Phi^T \boldsymbol{K} \Phi \boldsymbol{U}_r - \Phi^T \boldsymbol{P} = 0 \tag{13}$$

or

$$\boldsymbol{K}_r \boldsymbol{U}_r = \boldsymbol{P}_r \tag{14}$$

where

$$\boldsymbol{M}_r = \Phi^T \boldsymbol{M} \Phi, \qquad \boldsymbol{K}_r = \Phi^T \boldsymbol{K} \Phi, \qquad \boldsymbol{P}_r = \Phi^T \boldsymbol{P} \tag{15}$$

Note that not all solutions of Eq. (5) are necessarily solutions of Eq. (14). Rather, the reduced problem captures only the symmetric solution points of Eq. (6).

The analytical steps for obtaining the static response of symmetric incremental nonlinear problems can be described as follows:

1) Compute the out-of-balance load vector $\Delta \boldsymbol{P}$.

2) Set up the reduced symmetry subspace under the basis vector Φ. Obtain the reduced stiffness matrix and the reduced out-of-balance force vector as $\boldsymbol{K}_r = \Phi^T \boldsymbol{K} \Phi$, $\Delta \boldsymbol{P}_r = \Phi^T \Delta \boldsymbol{P}$.

3) Solve the incremental displacements under the subspace. This computation involves solving the reduced system $\boldsymbol{K}_r \Delta \boldsymbol{U}_r = \Delta \boldsymbol{P}_r$ for generalized incremental displacement vector $\Delta \boldsymbol{U}_r$ using the displacement control technique.

4) Obtain the original full-space incremental nodal displacement vector using $\Delta \boldsymbol{U} = \Phi \Delta \boldsymbol{U}_r$.

5) Update the nodal coordinates.

6) Compute new member forces.

7) Repeat steps 1 through 6. Computation stops when energy convergence criteria are met.

Optimization Criterion

The optimization problem is defined in the following form: Minimize the mass

$$M = \sum_{i=1}^{n} \rho_i A_i L_i \tag{16}$$

subject to

$$g = \Pi - \bar{\Pi} = 0 \tag{17}$$

where ρ_i, A_i, L_i, and n are the material density of the ith element, the cross-sectional area of the ith element (design variable), the deformed length of the ith element, and the number of truss elements, respectively. Π is the total potential energy, and $\bar{\Pi}$ is the target total potential energy associated with the optimum design at the limit load.

The effect of nonlinear buckling constraint is considered implicitly in the equality constraint given by Eq. (17). In other words, at the end of the nonlinear buckling analysis for each optimization iteration, the total potential energy is obtained. This total potential energy represents the potential energy of the system at the limit point. Thus, it may be said that the constraint on the limit load is equivalent to the constraint on the total potential energy of the system at the limit load.

The potential energy of a structure, made up of n elements, may be expressed as

$$\Pi = \sum_{i=1}^{n} U_i - \boldsymbol{U}^T \boldsymbol{P} = U - \boldsymbol{U}^T \boldsymbol{P} \tag{18}$$

where $\boldsymbol{U}$ is the global displacement vector, $\boldsymbol{P}$ is the vector of the externally applied forces , U is the total strain energy, and U_i is the strain energy of a typical ith element. For one-dimensional elements, it can be expressed as

$$U_i = \tfrac{1}{2} E_i \varepsilon_i^2 A_i L_i \tag{19}$$

where E_i is the module of elasticity of the ith element and ε_i is the strain in the ith element, expressed as

$$\varepsilon_i = (L_i - L_{0i})/L_{0i} \tag{20}$$

where L_{0i} is the undeformed length of the ith element. Invoking the principle of stationary total potential energy,

$$f\Pi / f\boldsymbol{U} = (fU / f\boldsymbol{U}) - \boldsymbol{P} = 0 \tag{21}$$

Using Eqs. (16) and (17), the Lagrangian L may be written as

$$L = \sum_{i=1}^{n} \rho_i A_i L_i - \lambda(\Pi - \bar{\Pi}) \tag{22}$$

where λ is a Lagrange multiplier. The Karush–Kuhn–Tucker (KKT) conditions for minimization of L with respect to A_i and λ, according to Eq. (22), become

$$\rho_i L_i - \lambda\left(\frac{\partial \Pi}{\partial A_i} + \sum_{j=1}^{m} \frac{\partial \Pi}{\partial U_j}\frac{\partial U_j}{\partial A_i}\right) = 0, \qquad (\Pi - \bar{\Pi}) = 0 \tag{23}$$

where m is the number of displacement DOF. By virtue of Eq. (21), corresponding to every nodal displacement U_j, $f\Pi/fU_j$ vanishes, and hence Eq. (23) may be written as

$$\rho_i L_i - \lambda(f\Pi/fA_i) = 0 \tag{24}$$

Considering Eqs. (18) and (19) , we have

$$f\Pi/fA_i = U_i/A_i \tag{25}$$

Substituting Eq. (25) into Eq. (24) gives

$$\rho_i L_i - \lambda(U_i/A_i) = 0 \tag{26}$$

or

$$\lambda \hat{U}_i = 1 \tag{27}$$

where $\hat{U}_i = U_i/\rho_i L_i A_i$ is the strain energy density of the ith element. Equation (27) is an optimality criterion and states that in an optimum structure, the strain energy density is equal for all elements.

Recurrence Relation

To obtain a design that satisfies the optimality criterion given by Eq. (27), an iterative scheme is used. This consists of updating the design variables using the recurrence relation, or alternatively the design variable update formulas, after determining the nonlinear critical point. A simple and efficient form of the recurrence relation may be expressed by multiplying both sides of Eq. (27) by $(A_i)^{\beta}$ and taking its βth root as

$$A_i^{v+1} = A_i^v(\lambda \hat{U}_i)_v^{1/\beta} \tag{28}$$

where $v+1$ and v are the iteration steps. The step-size parameter β controls the convergence rate and can be changed by assigning appropriate values. Using the recurrence relation in Eq. (28), in each optimization iteration the design variables are updated until the relative convergence criteria are satisfied. It is noted that the final optimum design is not influenced by the step-size parameter because $\lambda\hat{U}$ is equal to unity in the final optimum design. Selecting large step-size parameter results in a slow and smooth convergence and a large number of optimization iterations before satisfying the convergence criteria. Conversely, choosing a small step-size parameter results in a fast and oscillating convergence so that the required convergence criteria may never be reached. It is recommended that the step-size parameter be set to a small number (4 has been selected for the present design) and then increased gradually as the optimization process evolves.

To use Eq. (28), it is required to know the value of the Lagrange multiplier λ. At the optimal design, λ will satisfy Eq. (27). For nonoptimal design, a value of λ that most closely satisfies this equation is needed. In nonoptimal design, consider a residual Res defined as

$$Res_i = 1 - \lambda \hat{U}_i \tag{29}$$

Now λ is taken as the value that minimizes the sum of the squares of the residuals, that is, the value for which

$$\frac{\mathrm{d}}{\mathrm{d}\lambda}\left[\sum_{i=1}^{n} Res_i^2\right] = 0 \tag{30}$$

Equation (30) results in the following closed-form solution for the value of λ:

$$\lambda = \frac{\sum_{i=1}^{n} \hat{U}_i}{\sum_{i=1}^{n} \hat{U}_i^2} \tag{31}$$

Substituting Eq. (31) into Eq. (28), we finally obtain the following recurrence relation for updating the design variables:

$$A_i^{v+1} = A_i^v\left(\left[\frac{\sum_{i=1}^{n} \hat{U}_i}{\sum_{i=1}^{n} \hat{U}_i^2}\right]\hat{U}_i\right)_v^{1/\beta} \tag{32}$$

In the structure studied in this paper, the specified load on the structure must be equal to the nonlinear critical load of the structure. If this condition is satisfied at the end of each iteration, then every design will be a feasible one. This can be achieved by scaling the design following the analysis phase in the iteration cycle.

Scaling Procedure

After finding the limit load using the nonlinear buckling analysis at each optimization iteration, the design variables are scaled to the feasible region to satisfy the design constraint. In other words, the design limit load (P_{design}) of the structure must be equal to the limit load (P_{cr}) of the structure after the analysis phase in the iteration cycle. For truss elements, the strain energy is a linear function of the design variables; therefore, scaling the areas of all the members of the structure by a factor Sf has the effect of scaling the limit load P_{cr} by the same scale factor Sf, with no change in the displacement pattern. The scale factor for truss elements may be given by

$$Sf = P_{\text{design}}/P_{\text{cr}} \tag{33}$$

Illustrative Example: Space Dome Truss Structure

The complex space dome structure shown in Fig. 2 consists of 24 bars, and the 6 vertices are fixed so that there are 7 nodes free to move with total 21 DOF. This structure has six equivalent configurations corresponding to rotating the structure through the angles $n\pi/3$; $n = 0, 1, \ldots, 5$ and six equivalent configurations corresponding to the reflection of the structure with respect to the plane through the Z axis and the line through the origin in the X–Y plane that makes a counterclockwise angle of $n\pi/6$; $n = 0, 1, \ldots, 5$ with the X axis.

In the Cartesian coordinate system, the X, Y, and Z axes are shown in Fig. 2. Each of the preceding actions can be represented by a $3 \leftrightarrow 3$ orthogonal rotation or reflection matrix. The rotation spanning a counterclockwise angle θ about the Z axis from the global coordinate system to the local axes system for the members is given by

$$\boldsymbol{R} = \begin{bmatrix} \cos\theta & -\sin\theta & 0 \\ \sin\theta & \cos\theta & 0 \\ 0 & 0 & 1 \end{bmatrix} \tag{34}$$

The reflection across a plane perpendicular to the X–Y plane that makes a counterclockwise angle of $\theta/2$ with the X–Z plane is given by

$$\boldsymbol{S} = \begin{bmatrix} \cos\theta & \sin\theta & 0 \\ \sin\theta & -\cos\theta & 0 \\ 0 & 0 & 1 \end{bmatrix} \tag{35}$$

The complete symmetry group of the structural configuration is the set of all orthogonal transformations that map the system into an equivalent configuration and are given by

$$\boldsymbol{T}_1 = \boldsymbol{R}(0)(\boldsymbol{U}_1, \boldsymbol{U}_2, \boldsymbol{U}_3, \boldsymbol{U}_4, \boldsymbol{U}_5, \boldsymbol{U}_6, \boldsymbol{U}_7)$$

$$\boldsymbol{T}_2 = \boldsymbol{R}(60)(\boldsymbol{U}_2, \boldsymbol{U}_5, \boldsymbol{U}_1, \boldsymbol{U}_4, \boldsymbol{U}_7, \boldsymbol{U}_3, \boldsymbol{U}_6)$$

$$\boldsymbol{T}_3 = \boldsymbol{R}(120)(\boldsymbol{U}_5, \boldsymbol{U}_7, \boldsymbol{U}_2, \boldsymbol{U}_4, \boldsymbol{U}_6, \boldsymbol{U}_1, \boldsymbol{U}_3)$$

$$\boldsymbol{T}_4 = \boldsymbol{R}(180)(\boldsymbol{U}_7, \boldsymbol{U}_6, \boldsymbol{U}_5, \boldsymbol{U}_4, \boldsymbol{U}_3, \boldsymbol{U}_2, \boldsymbol{U}_1)$$

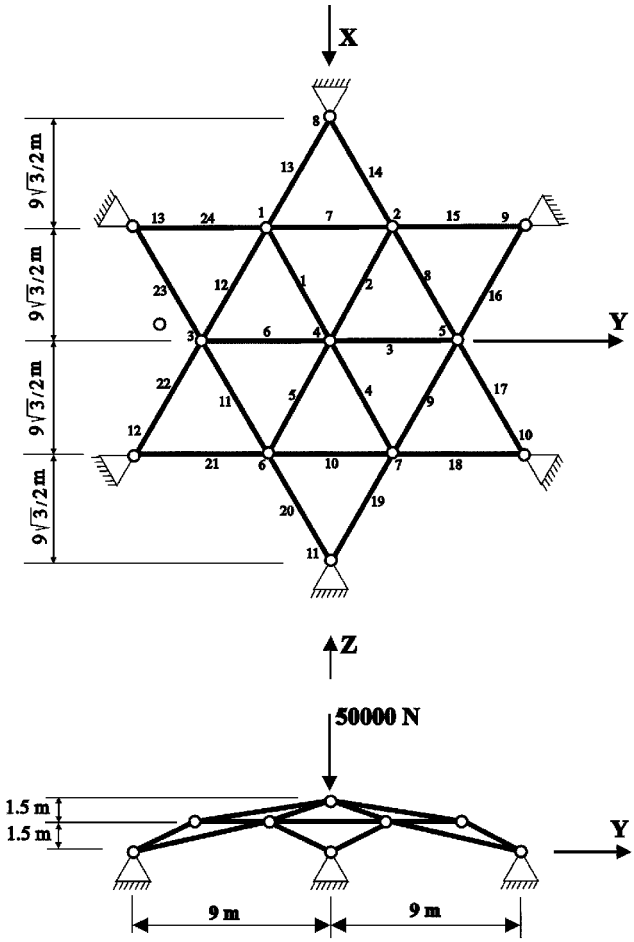

Fig. 2 Twenty-four-bar space dome structure.

$$\boldsymbol{T}_5 = \boldsymbol{R}(240)(\boldsymbol{U}_6, \boldsymbol{U}_3, \boldsymbol{U}_7, \boldsymbol{U}_4, \boldsymbol{U}_1, \boldsymbol{U}_5, \boldsymbol{U}_2)$$

$$\boldsymbol{T}_6 = \boldsymbol{R}(300)(\boldsymbol{U}_3, \boldsymbol{U}_1, \boldsymbol{U}_6, \boldsymbol{U}_4, \boldsymbol{U}_2, \boldsymbol{U}_7, \boldsymbol{U}_5)$$

$$\boldsymbol{T}_7 = \boldsymbol{S}(0)(\boldsymbol{U}_2, \boldsymbol{U}_1, \boldsymbol{U}_5, \boldsymbol{U}_4, \boldsymbol{U}_3, \boldsymbol{U}_7, \boldsymbol{U}_6)$$

$$\boldsymbol{T}_8 = \boldsymbol{S}(60)(\boldsymbol{U}_1, \boldsymbol{U}_3, \boldsymbol{U}_2, \boldsymbol{U}_4, \boldsymbol{U}_6, \boldsymbol{U}_5, \boldsymbol{U}_7)$$

$$\boldsymbol{T}_9 = \boldsymbol{S}(120)(\boldsymbol{U}_3, \boldsymbol{U}_6, \boldsymbol{U}_1, \boldsymbol{U}_4, \boldsymbol{U}_7, \boldsymbol{U}_2, \boldsymbol{U}_5)$$

$$\boldsymbol{T}_{10} = \boldsymbol{S}(180)(\boldsymbol{U}_6, \boldsymbol{U}_7, \boldsymbol{U}_3, \boldsymbol{U}_4, \boldsymbol{U}_5, \boldsymbol{U}_1, \boldsymbol{U}_2)$$

$$\boldsymbol{T}_{11} = \boldsymbol{S}(240)(\boldsymbol{U}_7, \boldsymbol{U}_5, \boldsymbol{U}_6, \boldsymbol{U}_4, \boldsymbol{U}_2, \boldsymbol{U}_3, \boldsymbol{U}_1)$$

$$\boldsymbol{T}_{12} = \boldsymbol{S}(300)(\boldsymbol{U}_5, \boldsymbol{U}_2, \boldsymbol{U}_7, \boldsymbol{U}_4, \boldsymbol{U}_1, \boldsymbol{U}_6, \boldsymbol{U}_3) \tag{36}$$

in which $\boldsymbol{R}(\theta)$ and $\boldsymbol{S}(\theta)$ are defined by Eqs. (34) and (35) and $\boldsymbol{U}_i$ is the displacement vector of the ith node. For example, $\boldsymbol{T}_2$ has the following form:

$$\boldsymbol{T}_2 = \boldsymbol{R}(60)(\boldsymbol{U}_2, \boldsymbol{U}_5, \boldsymbol{U}_1, \boldsymbol{U}_4, \boldsymbol{U}_7, \boldsymbol{U}_3, \boldsymbol{U}_6)$$

$$= \begin{bmatrix} \mathbf{0} & \boldsymbol{R}(60) & \mathbf{0} & \mathbf{0} & \mathbf{0} & \mathbf{0} & \mathbf{0} \\ \mathbf{0} & \mathbf{0} & \mathbf{0} & \mathbf{0} & \boldsymbol{R}(60) & \mathbf{0} & \mathbf{0} \\ \boldsymbol{R}(60) & \mathbf{0} & \mathbf{0} & \mathbf{0} & \mathbf{0} & \mathbf{0} & \mathbf{0} \\ \mathbf{0} & \mathbf{0} & \mathbf{0} & \boldsymbol{R}(60) & \mathbf{0} & \mathbf{0} & \mathbf{0} \\ \mathbf{0} & \mathbf{0} & \mathbf{0} & \mathbf{0} & \mathbf{0} & \mathbf{0} & \boldsymbol{R}(60) \\ \mathbf{0} & \mathbf{0} & \boldsymbol{R}(60) & \mathbf{0} & \mathbf{0} & \mathbf{0} & \mathbf{0} \\ \mathbf{0} & \mathbf{0} & \mathbf{0} & \mathbf{0} & \mathbf{0} & \boldsymbol{R}(60) & \mathbf{0} \end{bmatrix} \tag{37}$$

where $\mathbf{0}$ is a 3×3 null matrix.

By using Eq. (9), the dimension of the symmetry-reduced subspace for the 24-bar space dome structure is

Table 1 Basis vectors spanning the symmetry subspace of the space dome

ϕ_1	ϕ_2	ϕ_3
0.000000	0.000000	0.353553
0.000000	0.000000	0.204124
0.000000	0.408248	0.000000
0.000000	0.000000	0.353553
0.000000	0.000000	−0.204124
0.000000	0.408248	0.000000
0.000000	0.000000	0.000000
0.000000	0.000000	0.408248
0.000000	0.408248	0.000000
0.000000	0.000000	0.000000
0.000000	0.000000	0.000000
1.000000	0.000000	0.000000
0.000000	0.000000	0.000000
0.000000	0.000000	−0.408248
0.000000	0.408248	0.000000
0.000000	0.000000	−0.353553
0.000000	0.000000	0.204124
0.000000	0.408248	0.000000
0.000000	0.000000	−0.353553
0.000000	0.000000	−0.204124
0.000000	0.408248	0.000000

$$m_r = \tfrac{1}{12}(21+2+0-1+0+2+3+1+3+1+3+1) = 3 \tag{38}$$

and, finally, substituting Eq. (36) into Eq. (7), the projection operator ($\boldsymbol{Pr}$) is promptly obtained. The eigenvectors of $\boldsymbol{Pr}$ corresponding to an eigenvalue of unity, according to Eq. (8), can be obtained by an eigenvector extraction algorithm. Because $m_r = 3$, there are three eigenvectors:

$$\Phi = [\phi_1 \quad \phi_2 \quad \phi_3] \tag{39}$$

These eigenvectors represent the basis vectors that span the symmetry subspace, and they are listed in Table 1. Note that in this problem, 21 DOF in the original full space are reduced to three-dimensional symmetry subspace.

Analysis

Using the displacement control technique, the nonlinear buckling analysis of both the full space and the reduced subspace are performed to obtain the limit load and illustrate the application of the GTA in nonlinear buckling analysis via the displacement control method. The Young's modulus and cross-sectional area for all members are assumed to be $E = 73 \times 10^{11}$ N/m^2 and $A = 5$ cm^2, respectively.

The downward vertical displacement in the apex (W) of the structure (node 4) is selected as the controlling displacement, and it is incremented in steps of 0.01 m per time step.

Figure 3 shows the nonlinear buckling analysis until limit load in both full space and reduced subspace for the 24-bar space dome. There is excellent agreement between full space and reduced subspace. The limit load has been obtained with an accuracy of 10^{-5} using the quadratic curve fit on the region close to the limit load. This method enables the controlling displacement to be incremented in smaller step size near the limit point. In both full space and reduced subspace, the limit load was found to be 111,729.2 N. The number of iterations to catch the limit point in both full space and subspace is 85. The computational time using the reduced subspace was about five times less than that of full-space analysis.

Figure 4 shows the postbuckling solution path using the displacement control technique in both full space and reduced subspace. The reduced subspace solution is in perfect agreement with the full-space solution for the postbuckling trajectory. Again, it was observed that the computational time for the subspace solution was about four times less than that of full-space analysis.

Optimization

The structure has been optimized previously, using the optimality criterion algorithm. The material is assumed to be aluminum, with Young's modulus $E = 73 \times 10^{11}$ N/m^2 and material density

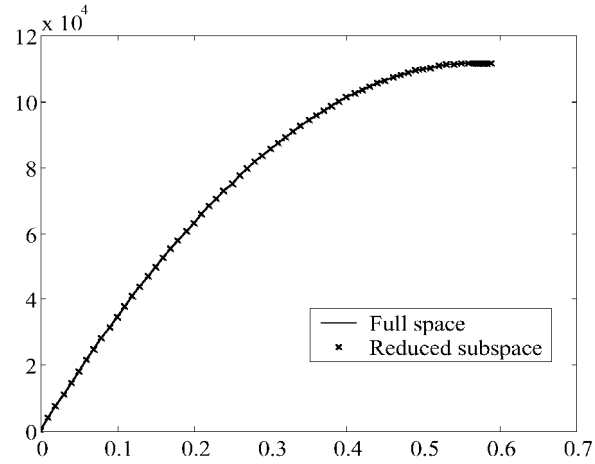

Fig. 3 Load-deflection curve for 24-bar space dome until limit load.

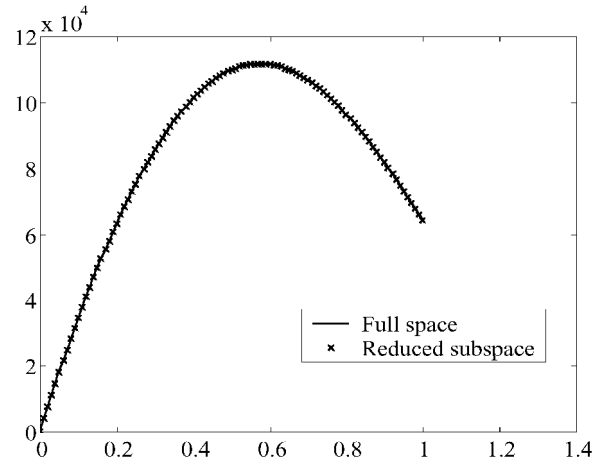

Fig. 4 Load-deflection curve for 24-bar space dome (postbuckling).

Table 2 Variable linking groups

Group	Elements
1	1–6
2	7–12
3	13–24

Table 3 Final designs for the area of cross-section (cm^2)

Group	Nonlinear buckling, full space	Nonlinear buckling, reduced subspace
1	2.6544	2.6548
2	1.7481	1.7484
3	0.9082	0.9083
Mass, kg	93.774	93.784
Iteration no.	19	17

Table 4 Final designs for the area of cross-section (cm^2)

Group	Linear buckling, optimization criterion algorithm	Linear buckling, SQP method
1	0.7407	0.5069
2	0.5000	0.5932
3	0.5000	0.5000
Mass, kg	33.874	31.725
Iteration no.	17	47

Table 5 Initial and final relative energy density distribution (nonlinear buckling)

Group number	Initial design	Final design (full space)	Final design (reduced subspace)
1	1	1.0000	0.9994
2	0.4841	1.0000	1.0000
3	0.0930	1.0000	0.9981

$\rho = 2770$ kg/m^3. The minimum area for all elements was set at 0.5 cm^2. The minimum size constraint was treated as a passive constraint. If the recurrence relation reduced the area of any element to a value smaller than the minimum specified, then the cross-sectional area of that element was set to the minimum size.

The structure was designed for a load of 50,000 N applied downward at node 4. The downward vertical displacement at this node was taken as the controlling displacement for the displacement control method, and it is incremented in steps of 0.01 m per displacement step. The stop criterion was selected to be $(m_{i+1} - m_i) = 10^{-5} m_{i+1}$, where m_{i+1} and m_i are masses of the structure in the iteration $(i+1)$th and ith.

To maintain the symmetry during the optimization, the elements have been linked into three groups, as shown in the Table 2.

The initial cross-sectional area for all elements was selected as 5 cm^2. The initial mass is 302.255 kg. With this initial area, the limit point obtained was 111,729.2 N. Therefore, the initial design is not in a feasible region (limit load is not equal to the design load of 50,000 N). The final design for cross-sectional areas through full space and reduced subspace using the GTA is shown in Table 3. It was observed that there is excellent agreement between the final designs using both the full space and the reduced subspace analysis. The computational time required by the reduced subspace analysis was found to be five times less than that of the full-space analysis.

Table 4 shows the optimization results when the system stability constraint is considered as the linear buckling analysis, which is a generalized eigenvalue analysis for the buckling load. Using the current optimality algorithm, in the final design, the strain energy was not equal in all elements and final weight of 33.874 kg was obtained, indicating that the optimum solution may not have been reached. To find out the possible optimum solution, the problem with the linear buckling constraint was solved again through the sequential quadratic programming (SQP) method, with the same initial area. The weight was reduced to 31.725 kg. Therefore, the optimum solution obtained by the optimality algorithm is not an optimum solution, although it is close to an optimum solution. We can say that if the final strain energy is not equal in the final design, we should cautiously check the design with other optimization methods for confirmation of the design. It is clear from Table 3 that there is significant difference in the number iteration and flops using the current optimization criterion and SQP, indicating that the current optimization criterion is more efficient than SQP.

Comparing the optimum mass based on the nonlinear buckling analysis (Table 3) with the solution based on the linear buckling analysis (Table 4), it is observed that the design based on the linear buckling underestimates the optimum mass by a factor of about 3, indicating that designs based on linear buckling analysis may be prone to failure.

Table 5 shows the relative strain energy in the initial design and final design for both the full-space and the reduced subspace solutions. It is noted that, in the initial design, the strain energy is not uniform for the elements. However, following the optimization process, the strain energy becomes exactly uniform in all elements for the full-space solution, showing that it has exactly reached the optimum point. On the other hand, using the reduced subspace, the strain energy does not become exactly uniform in all elements but very close to uniform. The small discrepancy between the final cross-sectional areas from the full-space and reduced subspace solutions is primarily due to round-off errors in analysis for the reduced subspace solution. Also, the basis vectors or projection matrix may induce errors in finding the exact limit point that is critical for obtaining the accurate optimum solution. Figure 5 shows the iteration history in both full space and reduced subspace, and it is noted that there is an excellent agreement throughout the iteration history.

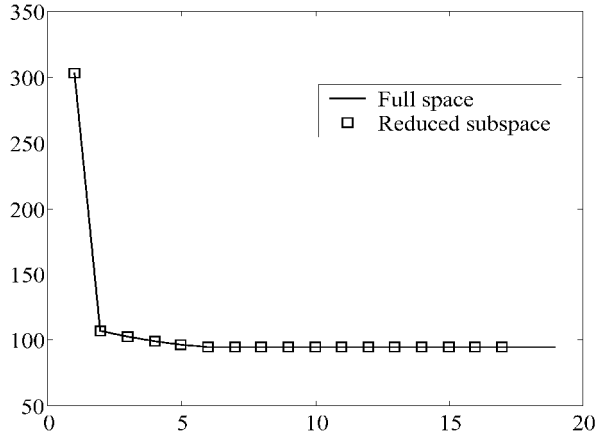

Fig. 5 Iteration history through full space and reduced subspace.

Conclusions

Nonlinear buckling analysis of geometrically nonlinear symmetric structures based on the displacement control technique in conjunction with the GTA is an efficient tool for stability analysis. Results obtained by the reduced subspace using the GTA are in excellent agreement with full-space solutions for limit load, prebuckling, and postbuckling path analysis of the load-deflection curve.

The nonlinear buckling analysis, based on the displacement control technique together with the GTA, has been applied to the structural optimization of a shallow, symmetric, space dome truss structure. It has been shown that the combination of the displacement control method using the GTA together with the optimality criterion, based on a uniform-strain energy density distribution, can be used effectively for the design of truss structures under system stability constraint. It has been demonstrated that structural optimization of nonlinear symmetric structures using the GTA can significantly reduce the computational effort, and excellent agreement exists between the optimum results from full space and the reduced subspace.

Finally, it was illustrated that designs based on the generalized eigenvalue problem (linear buckling) may considerably underestimate the optimum mass, which may lead to potential structural failure.

References

[1]Kiusalaas, J., "Optimal Design of Structures with Buckling Constraints," *International Journal of Solids and Structures*, Vol. 9, No. 7, 1973, pp. 863–878.

[2]Khot, N. S., "Nonlinear Analysis of Optimized Structure with Constraints on System Stability," *AIAA Journal*, Vol. 21, No. 8, 1983, pp. 1181–1186.

[3]Levy, R., and Perng, H. S., "Optimization for Nonlinear Stability," *Computers and Structures*, Vol. 30, No. 3, 1988, pp. 529–535.

[4]Levy, R., "Optimal Design of Trusses for Overall Stability," *Computers and Structures*, Vol. 53, No. 5, 1994, pp. 1133–1138.

[5]Khot, N. S., and Kamat, M. P., "Minimum Weight Design of Truss Structures with Geometric Nonlinear Behavior," *AIAA Journal*, Vol. 23, No. 1, 1985, pp. 139–144.

[6]Kamat, M. P., and Raungasilasingha, P., "Optimization of Space Truss Against Instability Using Design Sensitivity Derivatives," *Engineering Optimization*, Vol. 8, 1985, pp. 177–188.

[7]Smaoui, H., and Schmit, L. A., "An Integrated Approach to the Synthesis of Geometrically Nonlinear Structures," *International Journal for Numerical Methods in Engineering*, Vol. 26, No. 3, 1988, pp. 555–570.

[8]Kamat, M. P., Khot, N. S., and Venkayya, V. B., "Opimization of Shallow Trusses Against Limit Point Instability," *AIAA Journal*, Vol. 22, No. 3, 1984, pp. 403–408.

[9]Levy, R., "Optimization for Buckling with Exact Geometries," *Computers and Structures*, Vol. 53, No. 5, 1994, pp. 1139–1144.

[10]Zienkiewicz, O. C., "Incremental Displacements in Nonlinear Problems," *International Journal for Numerical Methods in Engineering*, Vol. 3, No. 4, 1971, pp. 587–592.

[11]Thomas, G., and Gallagher, R. H., "A Triangular Thin Shell Finite Element: Nonlinear Analysis," NASA CR-2483, 1975.

[12]Haisler, W. E., Stricklin, J. A., and Key, J. E., "Incrementation in Nonlinear Structural Analysis by Self-Correcting Method," *International Journal for Numerical Methods in Engineering*, Vol. 11, No. 1, 1977, pp. 3–10.

[13]Batoz, J. L., and Dhatt, G., "Incremental Displacement Algorithms for Nonlinear Problems," *International Journal for Numerical Methods in Engineering*, Vol. 14, No. 8, 1979, pp. 1262–1267.

[14]Sedaghati, R., and Tabarrok, B., "Optimum Design of Truss Structures Undergoing Large Deflections Subject to a System Stability Constraint," *International Journal for Numerical Methods in Engineering*, Vol. 48, No. 3, 2000, pp. 421–434.

[15]Sedaghati, R., Tabarrok, B., and Suleman, A., "Optimum Design of Nonlinear Symmetric Truss Structures Under System Stability Constraint," AIAA Paper 2000-4835, Sept. 2000.

[16]Bathe, K. J., *Finite Element Procedures*, Prentice–Hall, Englewood Cliffs, NJ, 1996.

[17]Healey, T. J., "Symmetry, Bifurcation and Computational Methods in Nonlinear Structural Mechanics," Ph.D. Dissertation, Dept. of Mechanical Engineering, Univ. of Illinois, Champaign, IL, 1985.

[18]Healey, T. J., "Symmetry and Equivariance in Nonlinear Elastostatics, Part I," *Archive for Rational Mechanics and Analysis*, Vol. 105, 1989, pp. 205–228.

[19]Healey, T. J., "A Group Theoretic Approach to Computational Bifurcation Problems with Symmetry," *Computer Methods in Applied Mechanics and Engineering*, Vol. 67, No. 3, 1988, pp. 257–297.

[20]Miller, W., Jr., *Symmetric Groups and Their Applications*, Academic Press, New York, 1972.

[21]Chang, P., and Healey, T. J., "Computation of Symmetry Modes and Exact Reduction in Nonlinear Structural Analysis," *Computers and Structures*, Vol. 28, No. 2, 1988, pp. 135–142.

[22]Li, L., "Computational Nonlinear Static and Dynamic Analysis of Symmetric Structures by Using the Group Theoretic Approach," Ph.D. Dissertation, Dept. of Mechanical Engineering, Univ. of Western Ontario, London, ON, Canada, 1999.

[23]Kamat, M. P., "Optimization of Shallow Arches Against Instability Using Sensitivity Derivatives," *Finite Elements in Analysis and Design*, Vol. 3, 1987, pp. 277–284.

[24]Wu, C. C., and Arora, J. S., "Design Sensitivity Analysis and Optimization of Nonlinear Structural Response Using Incremental Procedures," *AIAA Journal*, Vol. 25, No. 8, 1987, pp. 1118–1125.

A. Messac
Associate Editor